

Received October 15, 2020, accepted November 8, 2020, date of publication November 17, 2020,  
date of current version November 30, 2020.

Digital Object Identifier 10.1109/ACCESS.2020.3038624

# Cognitive Multi-Point Free Space Optical Communication: Real-Time Users Discovery Using Unsupervised Machine Learning

FEDERICA AVETA<sup>ID1</sup>, (Member, IEEE), HAZEM H. REFAI<sup>ID1</sup>, (Member, IEEE),

AND PETER G. LOPRESTI<sup>ID2</sup>, (Member, IEEE)

<sup>1</sup>Department of Electrical Engineering, The University of Oklahoma, Tulsa, OK 74135, USA

<sup>2</sup>Department of Electrical Engineering, The University of Tulsa, Tulsa, OK 74104, USA

Corresponding author: Federica Aveta (aveta@ou.edu)

**ABSTRACT** Multi-user free-space optical communication (FSOC) is beginning to draw a significant attention for its ability to support increased system network capacity while using single receiving photodiode and satisfying size, weight, and power (SWaP) constraints imposed by space- and aerial-based mobile communication. Despite these advantages, support of multi-user capabilities cause increased system complexity due to accommodating heterogenous users communications with varying transmission and data rate requirements. Machine learning (ML) has recently been considered as a promising approach for introducing cognition into the network to mitigate some of the complexity. A cognitive method based on unsupervised ML was derived for estimating the number of users communicating and sharing time and bandwidth resources with a single-node receiver. A weighted clustering approach was introduced and experimentally validated when users received with similar amplitude information that results in underestimation. Obtained results confirmed that the proposed methodology was able to accurately differentiate the number of simultaneously transmitting users with accuracy greater than 92%—even in the presence of moderate atmospheric turbulence. An experimental analysis was conducted to determine data size and receiver sampling rate requirements for accurate estimation. Furthermore, an empirical model was derived to evaluate the effect of preamble signal length given a particular sampling rate on the accuracy of the estimation. The model was validated for up-to four users.

**INDEX TERMS** Clustering, Cognitive Optical Wireless Communication (OWC), free space optical communication (FSOC), machine learning (ML), multi-user, Number of Users' Estimation, sample size, sampling rate.

## I. INTRODUCTION

Free-space optics (FSO) technology is poised to alleviate the scarcity of radio frequency (RF) spectrum and data rate limitations inherent in RF systems [1]. FSO offers a high-bandwidth and naturally supports Gb/s data rates. This technology encodes information on visible and invisible light, and then transmits light beams into the atmosphere to establish license-free, directional, secure, and electromagnetic interference-immune networking [2], [3]. Recently available FSO solutions successfully demonstrated the feasibility of free-space optical communication (FSOC) to meet the increasing demand for wireless capacity of space- and

The associate editor coordinating the review of this manuscript and approving it for publication was Rentao Gu<sup>ID</sup>.

air-based networks. Project Loon—developed by Google X—established a network of high-altitude balloons traveling in the stratosphere to address internet connectivity scarcity for a significant portion of the world's unserved population [4]. FSOC was adopted for inter-balloon crosslink communication. This same technology is also gaining significant attention for space applications. NASA space communications and navigation (SCaN) recently developed and tested optical communication technology using lasers with their lunar laser communications demonstration (LLCD), utilizing a lunar orbit spacecraft terminal and three ground terminals with up to 622 Mbps transmission rate in uplink [5]. One downside of current FSOC systems is the need for strict pointing, acquisition and tracking (PAT) systems, which require bulky mechanical gimbals for maintaining link availability and

guaranteeing wide or omni-directional coverage [6]. PAT systems are known to violate mobile communication network size, weight and power (SWaP) requirements [7], [6]. To further advance optical wireless networking capabilities without affecting such restrictive SWaP specifications, omni-directional and multi-user communication should be provided [8]. Multi-user FSOC will fulfil the increase bandwidth, high-capacity and -density demands of future communication networks and will represent a leap from the current single user limitation. Accordingly, extensive research has been directed at investigating technologies and methods that enable high-capacity, multi-point FSOC systems. Efforts have primarily focused on developing an FSO omnidirectional transceiver [9]–[12] and on investigating signal processing and optical multiple access (O-MAC) techniques to support multi-user communication. Researchers in [13]–[16] introduced and experimentally demonstrated the effectiveness of two O-MAC techniques—and combinations thereof—in a multi-user FSOC link: 1) non-orthogonal multiple access (NOMA) and 2) independent component analysis (ICA), which is an unsupervised signal processing method. Results showed successful signal decoding when employing two and three independent laser sources that are sharing time and bandwidth resources at the transmitting side and a fiber bundle at the receiver side. Notably, all tested O-MAC techniques assumed that the number of transmitting users is known at the receiver side. This phenomenon does not necessarily hold true, however, in real and dynamic communication scenarios. As such, knowledge of number of concurrent transmissions shall be beneficial to adaptively select the proper O-MAC technique for signal separation and decoding. Consequently, it is highly desirable to utilize an intelligent and flexible omni-directional and multi-user FSO system providing a) autonomous and real-time number of communicating users detection; b) dynamic and autonomous O-MAC techniques selection; c) real-time dynamic adjustment of transmitting/receiving parameters; d) agile, on-demand diverse service requirement fulfillments; and e) autonomous transmitter/receiver add and drop [13]. Such functionalities will likely cause future multi-user FSO networks increased system complexity and heterogeneity with regard to communicating devices, varied transmission technologies, and diverse quality of service (QoS) requirements from each user [17].

Introducing self-configuration, self-optimization, and automated decision-making capabilities for supporting heterogeneous users and services presents a significant challenge for future optical wireless networks [17]–[20]. In this paper, we propose a methodology to embed intelligence at the physical layer (PHY) of a multi-point FSOC system. Our solution utilizes unsupervised machine learning (ML) for detecting the number of transmitting users necessary to perform real-time, dynamic, and autonomous O-MAC technique selection. Clustering analysis (e.g., K-mean, K-medoid, hierarchical, and fuzzy algorithms) was employed to estimate the number of concurrently transmitting users simultaneously

sharing bandwidth, time, and space resources by exploiting their amplitude information. Furthermore, a weighted analysis was proposed wherein users with identical amplitude information were received and number of transmitters was underestimated [21].

A crucial issue in ML algorithms is determining the amount of data needed to achieve a specific required performance (i.e., *sample complexity* [22]) [23]–[26]. In fact, data sets that require lengthy processing time or excessive memory represent a significant limiting factor for real-time applications, even though improved accurate performance is guaranteed. Required storage for many clustering algorithms is more than linear. For example, hierarchical clustering memory requires  $O(m^2)$ , where  $m$  is the number of data objects. Large dataset scalability for clustering algorithms has been investigated, and several solutions have been proposed in literature [20], [27]. Sample size and sampling rate effects were experimentally studied to determine user count estimation accuracy. Once the minimum number of samples—given receiver sampling rate to guarantee accurate user estimation was identified, an empirical model was derived. Using a fitting power-law model, the empirical equation aimed to forecast the number of detectable transmitting users when provided with the number of processed samples and the receiver sampling rate.

The novelty of the presented study is the development of a blind technique (namely user discovery algorithm) to identify number of simultaneous transmissions sharing allocation resources (time and frequency). The work detailed in this paper contributes to the field of optical wireless communication (OWC) in three primary ways. It 1) establishes an analytical model for user discovery to allow accurate implementation of NOMA protocol for future multi-user FSOC networks; 2) establishes a ML-based methodology for enhancing cognitive capabilities at the PHY layer—beyond existing designs into cognitive fiber-based networks—for future OWC systems; and 3) details extensive experimental testing, analysis, and validation conducted for diverse communication scenarios by clearly identifying system performance and limitations for real-time system design and implementation.

The balance of this paper is organized as follows. The next section presents related work on ML applications for introducing cognition and intelligence into optical networks. Section 3 describes the experimental setup used for the model derivation, and Section 4 introduces the mathematical formulation of the proposed methodology, along with the data pre-processing steps and model validation. This is accomplished through experimental analysis, including several communication scenarios. Section 5 presents the sample complexity analysis and the derived empirical model. Section 6 describes experimental validation of the sample complexity analysis presented in Section 5, albeit with an increased number of users. Section 7 details system limitations; and Section 8 concludes the paper and provides suggestions for future work.

## II. RELATED WORK

ML is a methodology that has been widely employed to introduce intelligence in the network, making it possible for systems to independently perform cognitive tasks. Researchers are currently focusing on embedding intelligence in the PHY- and network-layer domains in point-to-point, fiber-based optical communication networks [17]–[19]. Applications of ML at the PHY domain primarily include quality of transmission (QoT) estimation, modulation format recognition (MFR), and optical performance monitoring (OPM), to name just a few.

Optical communication system OPM has become crucial for ensuring robust and reliable system performance. This task consists of estimating physical parameters (e.g., bit-error rate [BER], optical signal-to-noise ratio [OSNR], polarization mode dispersion [PMD], chromatic dispersion [CD], Q-factor, and others) without prior knowledge from incoming optical signals for undertaking actions like adjusting transmitted power, re-routing traffic, and changing modulation format. Researchers in [28], [29] proposed using an artificial neural network (ANN) for simultaneous monitoring of OSNR, CD, and PMD. In [28], investigators trained the ANN using an asynchronous amplitude histogram. Simulation results for both 40 Gb/s return-to-zero differential quadrature phase-shift keying (RZ-DQPSK) and 40 Gb/s 16 quadrature amplitude modulation (16-QAM) systems demonstrated high monitoring accuracies. In [29], an ANN was trained using the first five empirical moments of the asynchronously sampled signal amplitude. Also, the first five empirical moments of the amplitude signal traversing through an offset fiber branch were added in the training phase to discriminate the sign of accumulated CD. Simulations in 40/56 Gb/s RZ-DQPSK and 40 Gb/s RZ-DPSK systems proved good simultaneous and independent in-band OSNR, signed CD, and PMD monitoring accuracy.

Researchers experimentally demonstrated the use of a deep neural network (DNN) for OSNR monitoring in [25], and the use of a convolutional neural network (CNN) for OSNR estimation and modulation format/symbol rate classification in [30]. Both experiments used asynchronously sampled raw data collected by a coherent receiver. NN input consisted of 512 samples x four channels corresponding to the horizontal (H) and vertical (V) polarization of the in-phase (I) and quadrature-phase (Q) components of the optical field (i.e., HI, HQ, VI and VQ). In [25], a five-layer DNN trained with 400,000 samples proved to successfully estimate OSNR in a 16 GBd dual-polarization quadrature phase-shift keying (DP-QPSK) with a measured averaged error of 1.6 dB. The CNN in [30] proved to successfully estimate OSNR in 14- and 16-GBd DP-QPSK, 16-QAM, and 64-QAM systems with mean square error (MSE) less than 0.3 dB for all the tested modulation formats. Classification accuracy >95% was achieved for modulation format/symbol rate classification.

MFR aims to estimate the modulation format at the receiver side—without prior information from the transmitters—for

improving signal demodulation accuracy and signal processing. Notably, some digital signal processing (DSP) algorithms used in a coherent receiver (e.g., adaptive equalization, carrier phase recovery and symbol detection) are modulation-format dependent. In [31], researchers experimentally demonstrated MFR in a 312.5 MBd QPSK, 8 phase shift keying (PSK), and 16-QAM system over 40 km single mode fiber (SMF) using a clustering technique. *K*-means algorithm was adopted to estimate number of clusters in the 2-dimensional I and Q constellation diagram. BER results proved successful demodulation for all tested modulation formats. Researchers in [32] implemented a simultaneous MFR and OSNR estimation using a CNN and eye-diagram as the processing objective. Eye-diagrams were simulated for a wide range of OSNR (e.g., 10 to 25 dB) and for four modulation formats, namely RZ-on off keying (OOK), non-return-to-zero NRZ-OOK, RZ-DPSK, and four-pulse amplitude modulation (4-PAM). 100% MFR accuracy was achieved with training data from 800 eye-diagrams, and 100% OSNR estimation was obtained after 31 epochs. Researchers in [33] used neural network (NN)-based nonlinear regression and a support vector machine (SVM) classifier to experimentally demonstrate independent in-band OSNR estimation and MFR. OSNR values ranged from 4 to 30 dB in four modulation formats, namely QPSK, 8-QAM, 16-QAM, and 64-QAM, which were experimentally tested. Eight features were extracted from the power eye-diagram (i.e., related to the mean values and variances at two points in the eye-diagram) of the directly-detected optical signals. One feature was used for NN training, and all features were employed for SVM. Results showed that the NN provided accurate OSNR estimation with mean estimation error of 0.7 dB; the classifier obtained an average classification accuracy of 94%.

QoT estimation in an optical connection consists of predicting some PHY parameters of a candidate light path as OSNR, BER, Q-factor, or another that might affect signal detection at the receiver side. Thus, these parameters represent a metric that should be measured, given that a required QoT is satisfied. In [26], a QoT estimation technique that considered both linear and nonlinear impairments was proposed. Synthetic BER data were calculated with varying total link length, span length values, channel input powers, data rate, and modulation formats. Three ML-based classifiers, namely Random Forest (RF), SVM, and K-Nearest Neighbor (KNN), were used to predict if light path BER will exceed a threshold. Results proved that SVM outperformed RF and KNN; 99.15% classification accuracy was achieved. Researchers in [23] proposed and experimentally validated an ANN-based transfer learning method for predicting the Q-factor in various optical transmission systems without re-training the all-ANN model.

ANN was trained in a four-span, large effective area fiber (LEAF) 100 Gb/s QPSK testbed, and then used to predict Q-factor in three optical systems: 1) four-span LEAF 200 Gb/s 16-QAM; 2) two-span LEAF 200 Gb/s 16-QAM; and 3) three-span dispersion-shifted fiber (DSF) 100 Gb/s

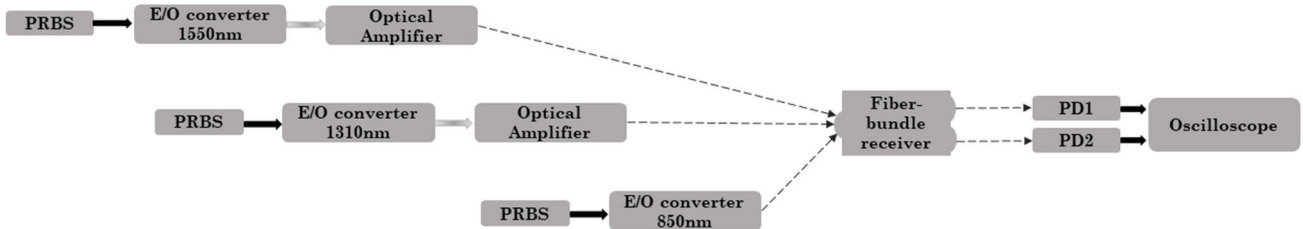
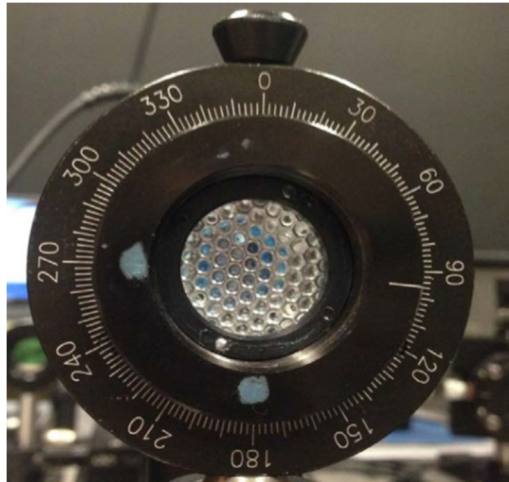
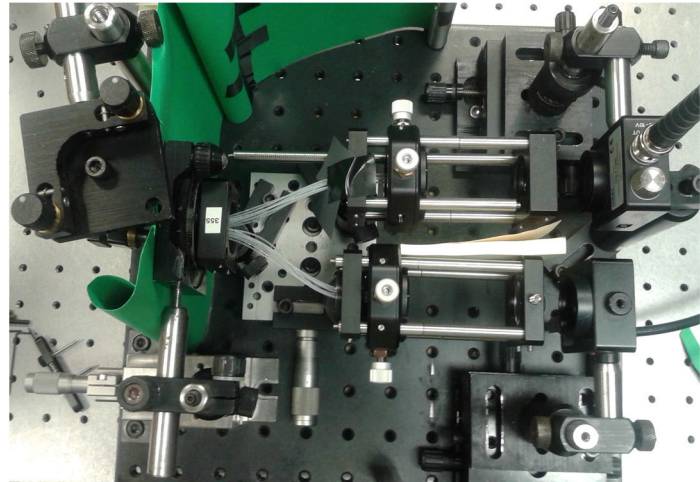


**FIGURE 1.** Depiction of the experimental setup.



(a)



(b)

**FIGURE 2.** Fiber bundle receiver: (a) front view; (b) top view.

QPSK. Only 20 training samples were added for each of the three tested optical systems and only weights of some hidden layers in ANN were tuned. A Q-factor prediction accuracy of 0.42 dB, 0.37 dB, and 0.67 dB was achieved, respectively, for the four-span LEAF 16-QAM, two-span LEAF 16-QAM, and three-span DSF QPSK systems.

### III. EXPERIMENTAL SETUP

The experimental setup used in this work is composed of three independent optical transmitters and a dual-path fiber bundle receiver (See Fig. 1). In the block diagram, the black lines connecting the blocks represent electrical links; the gray lines represent optical fiber connections; and the dashed lines represent free space optical links. Optical sources consisted of three electrical-to-optical converters with fiber-coupled laser diodes operating at three optical transmission wavelengths (e.g., 1550 nm, 1310 nm, and 850 nm). Although the transmitters employed three different wavelengths, no wavelength division multiplexing (WDM) was implemented (see photodiode specs—employed photodiode receives all three wavelengths as one) in this study. (The wavelength of each transmitter will be used throughout this manuscript as a label/identifier of the transmitter.) An intensity modulation (i.e., NRZ-OOK) with direct detection (IM/DD) scheme was employed for transmission. Laser sources were directly modulated by three independent, pseudo-random bit sequences (PRBS) that were  $2^{31}-1$  bits in

length. Data rate was experimentally proven up to 250 Mbps (See validation section VI). The 1550 nm optical output was connected to a doped fiber optical amplifier, and the 1310 nm to a semiconductor optical amplifier. No amplifier was implemented for the 850 nm source. Output power for each source was coupled with an optical telescope for collimating the propagating beams to the receiver. The dual-path fiber bundle receiver was composed of a hexagonal array of 19 small lenses—3 mm focal length—that couple the signal in an array of 19 multi-mode fibers—core diameter 400  $\mu$ m and numerical aperture of 0.37 [11] (See Fig. 2). The fiber bundle was implemented to greatly enhance the receiver’s field-of-view, while allowing the researchers to control signal path. The fibers split into two separate paths, with 10 fibers in one path, and 9 in the other. Fibers transmitted the signals to an array of graded index lenses, which collimated optical signals in two aspheric lenses—focal length of 20 mm and diameter of 25.4 mm. Array outputs were focused toward the collecting area of two photodetectors, namely Thorlabs PDA10CF (PD1: 800-1700 nm, 150 MHz BW) and PDA015C (PD2: 800-1700 nm, 380 MHz BW). Although three different wavelengths were implemented, the two photodiodes receive them as one signal, given no wavelength-based filtering employed. A 10° wedge prism was placed in front of the receiving lens array to vary the angle between the optical signals received by photodiode one and two. Fiber bundle design guaranteed a 10° wide field of view (FoV), making the receiver

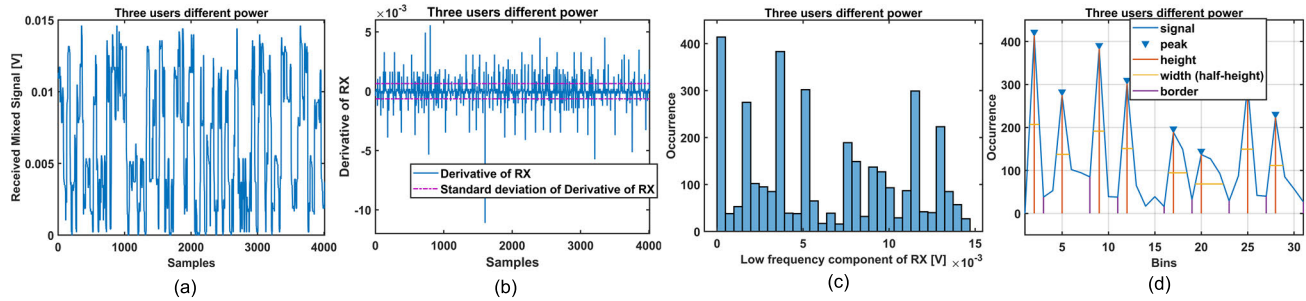


**FIGURE 3.** Three users different power: (a) Received mixed signal; (b) Derivative of received mixed signal; (c) 1-D histogram  $H_L[y_{LF}]$ ; (d) Peak detection of  $H_L[y_{LF}]$ .

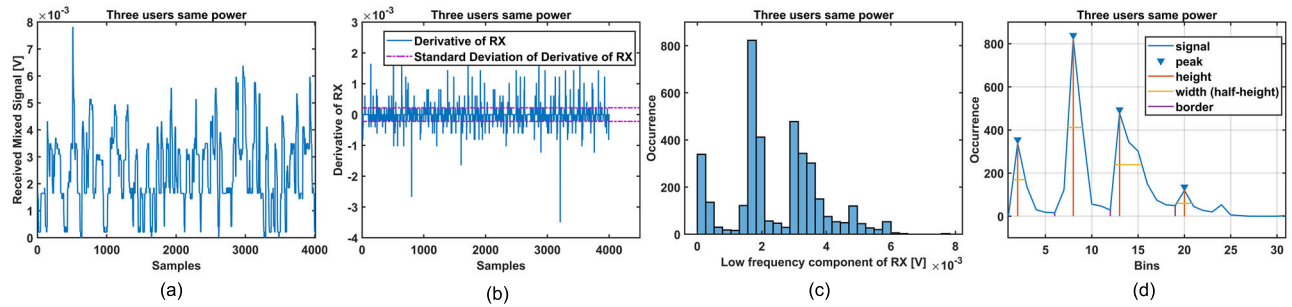


**FIGURE 4.** Three users same power: (a) Received mixed signal; (b) Derivative of received mixed signal; (c) 1-D histogram  $H_L[y_{LF}]$ ; (d) Peak detection of  $H_L[y_{LF}]$ .

suitable for multi-user communication analysis. Transmitter beam diameters were adjusted such that a) optical power of 1550 nm and 1310 nm laser sources coupled efficiently into photodetectors PD1 and PD2 and b) optical power of 850 nm laser source coupled efficiently into only photodetector PD2. Wavelength selective filters or wavelength demultiplexers were not implemented at the receiving side. Our experimentation validates the proposed method to accurately identify transmitting users sharing a receiver. A National Instruments virtual bench oscilloscope with sampling rate of 1 GSample/s was used to record data collected from the two photodetectors and the transmitted PRBS. Data analysis was performed after data collection using MATLAB software and the available statistical and ML MATLAB toolbox software equipped with a 2.60-GHz Intel Core i7 processor.

#### IV. USERS DISCOVERY ALGORITHM

A NRZ-OOK modulation was adopted as the scheme for this study. OOK is a binary level modulation format widely used in FSOC due to its simplicity and high-power efficiency [3]. When employing OOK with one user, two possible optical outputs are expected: 1)  $P_T$  (transmitted power) when “1” is transmitted and 2)  $\alpha_e P_T$  ( $\alpha_e$  = optical source extinction ratio  $0 \leq \alpha_e \leq 1$ ) when “0” is transmitted [34]. When  $N$  independent users simultaneously transmit, there will be  $k = 2^N$  possible optical power outputs. Hence,  $k$  power levels will be detected at the receiver side. Conversely, if  $k$  power measurements are detected, it is possible to retrieve the number of transmitting users as  $N = \log_2 k$ . Thus, we propose using unsupervised learning (i.e., clustering techniques) to extract power levels from the received mixed signals, and then

calculate the number of broadcasting users. The steps carried out in our proposed methodology are shown in Fig. 3 and 4. Data pre-processing was required to compute the number of expected clusters ( $K$ ) as input to clustering algorithms. Four clustering methods (e.g.,  $K$ -mean,  $K$ -medoid, hierarchical, and fuzzy) were subsequently evaluated. Moreover, a weighted clustering was developed to correct for user underestimation when received amplitudes a) were of equal power and b) equality  $N = \log_2 k$  was no longer valid. Although cases with one, two, and three transmitting users were analyzed, only three-user case scenario results will be shown hereafter.

#### A. PRE-PROCESSING

Pre-processing steps for three users received with varying power (See Fig. 3) and with the same power (See Fig. 4) are shown. A third-order median filter was applied on the received mixed signals to remove impulsive noise resulting from electrical devices or communication transmission [35]. Fig. 3(a) demonstrates an example of de-noised, received mixed signals for three users with different power levels and Fig. 4(a) with the same levels. Because we were interested in detecting power levels (i.e., constant power values) of transmitting users, low frequency components of the received signal (i.e., amplitude values changing slowly or slightly in the time domain) were considered. Numerical differentiation of the de-noised received mixed signal  $y[n]$  was performed, and the high- and low-frequency components of the data were extracted, as described in Eq. (1). Standard deviation of the first derivative of the received signal was set as a threshold.

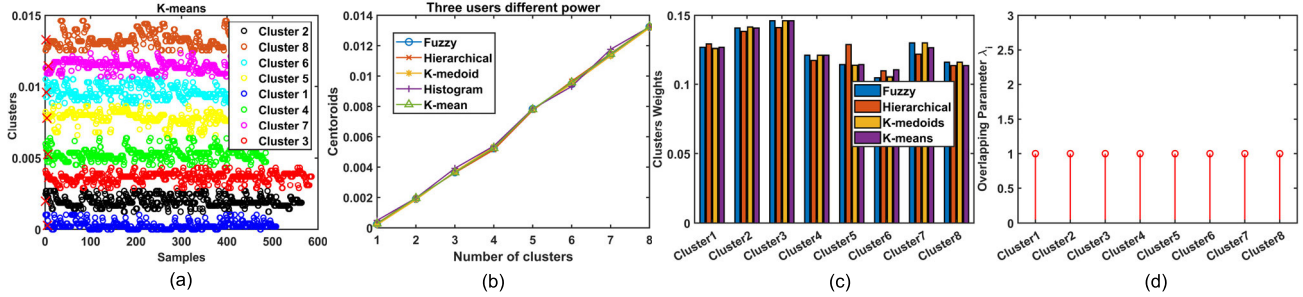


**FIGURE 5.** Three users different power: (a) K-means clustering results; (b) clusters centroids and histogram peaks; (c) cluster weights  $\rho_i$ ; (d) overlapping parameter  $\lambda_i$ .

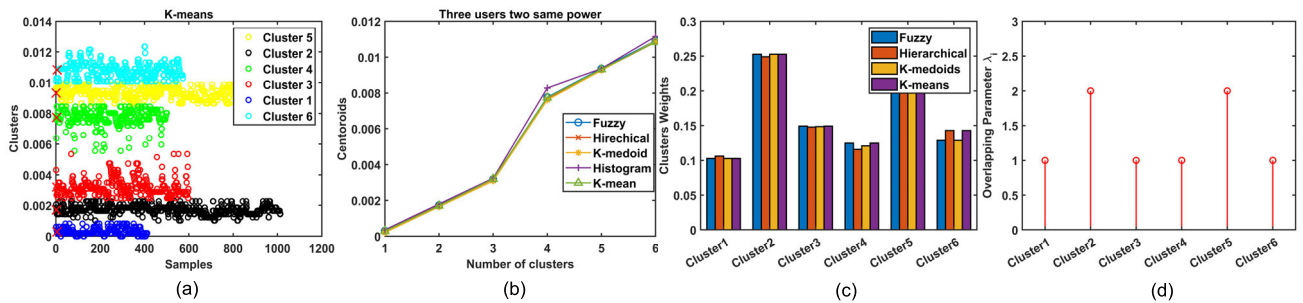


**FIGURE 6.** Three users two same power: (a) K-means clustering results; (b) clusters centroids and histogram peaks; (c) cluster weights  $\rho_i$ ; (d) overlapping parameter  $\lambda_i$ .

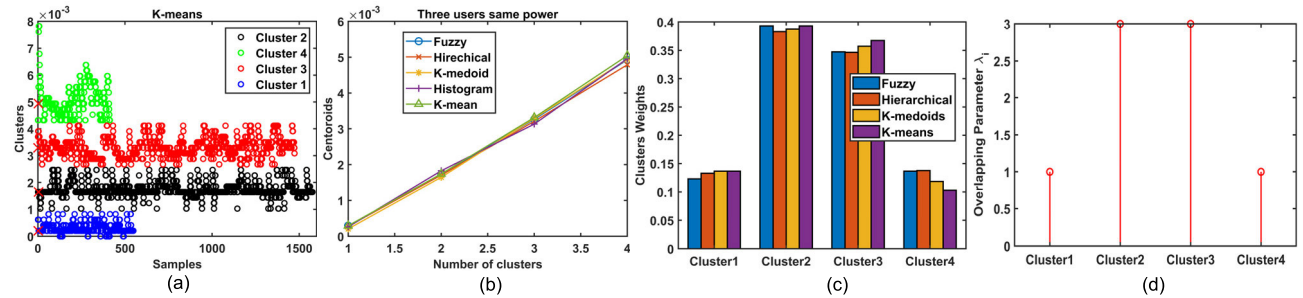


**FIGURE 7.** Three users same power: (a) K-means clustering results; (b) clusters centroids and histogram peaks; (c) cluster weights  $\rho_i$ ; (d) overlapping parameter  $\lambda_i$ .

See magenta dotted lines in Fig. 3(b) and Fig. 4(b).

$$y[n] = \begin{cases} y_{LF}[n] & \text{if } \frac{dy[n]}{dn} < \text{std}\left(\frac{dy[n]}{dn}\right) \\ y_{HF}[n] & \text{if otherwise} \end{cases} \quad (1)$$

Low frequency components of the signal  $y_{LF}[n]$  (i.e., received samples  $y[n]$  whose derivative fell within its standard deviation) were considered for the pre-processing analysis. To extract power levels, the occurrence of the signal's low frequency components were measured, and the empirical 1-D histogram  $H_L[y_{LF}]$  was computed, as illustrated in Fig. 3(c) and 4(c). Since we were interested in peak detection, local maxima of the  $H_L[y_{LF}]$  (i.e. more frequent power values [or levels]) were calculated following Eq. (2). See Fig. 3(d) and Fig. 4(d).

$$\arg \max H_L[y_{LF}] = p_m \quad (2)$$

$p_m$  is the peak position with integer  $m \in [1, \text{number of detected peaks}]$ ; number of peaks in the histogram was

expected to be  $m = k = 2^N$ . Thus, number of detected peaks was provided as input for the clustering algorithms as number of expected clusters. In the first case,  $m = 8$  was obtained validating  $m = k = 8 = 2^3$  (See Fig. 3[d]); whereas, in the second case,  $m = 4$  was obtained obtaining the inequality  $m \neq k = 2^3$ . (See Fig. 4[d]). As such, calculation of the local maxima of  $H_L[y_{LF}]$  does not suffice for correctly estimating number of concurrently transmitting users, given that a power control scheme was not implemented at the transmitting side. As such, a weighted clustering analysis was introduced to overcome user number underestimation.

## B. WEIGHTED CLUSTERING

$K$ -mean,  $K$ -medoid, hierarchical, and fuzzy clustering algorithms were applied on the low frequency components of the received mixed signal  $y_{LF}[n]$ . All methods were able to cluster data samples, as illustrated in Figures 5 through 7. However, given that a power allocation scheme was not

employed, and more than one user was transmitting with the same power, the results would have been an overlapping of the received signals in the power domain. This would lead to inequality  $m \neq k = 2^N$ . In fact, when two users transmit with the same power  $P_T$ , they will be clustered together, which leads to an underestimation of user number, as shown in Fig. 6 and Fig. 7. Thus, to evaluate if each cluster has more than one signal overlapped, each will be assigned weight  $\rho_i$ , defined as:

$$\rho_i = \frac{L_i}{L}, \quad 1 \leq i \leq K \quad (3)$$

where  $L$  is the total number of samples of the processed data;  $L_i$  is the number of samples belonging to cluster  $i$ ; and  $K$  is the total number of obtained clusters. Thus, weights  $\rho_i$  satisfy the following conditions.

$$\sum_{i=1}^K \rho_i = 1 \quad \text{and } 0 < \rho_i \leq 1 \quad (4)$$

As previously mentioned, given  $N$  transmitting users,  $k = 2^N$  possible outputs power are expected. Assuming that the probability of transmitting a “1” or a “0” is equally likely for all users, the probability of each possible output  $E_l$  with  $1 \leq l \leq k$  is equal to  $P(E_l) = \frac{1}{k} = \frac{1}{2^N}$ . Thus, the expected weight  $\hat{\rho}_i$  for each cluster, given no overlap in the power domain such that  $k = K$ , is expressed as:

$$\hat{\rho}_i = P(E_l) = \frac{1}{2^N} \quad 1 \leq i \leq K \text{ and } 1 \leq l \leq k \quad (5)$$

If the probability that users transmitting “0” will always be  $P(E_1) = \frac{1}{2^N}$ , regardless of their transmitting power, we can define the reference weight  $\hat{\rho}_1$  as the minimum weight obtained from Eq. 3:

$$\hat{\rho}_1 \approx P(E_1) = \min \{\rho_i\}_{i=1}^K \quad (6)$$

To identify the number of signals hidden in each cluster, we introduce an overlapping parameter  $\lambda_i$ , defined as the nearest integer of the ratio between the weights of each cluster  $\rho_i$  and the reference weight  $\hat{\rho}_1$ :

$$\lambda_i = \left[ \frac{\rho_i}{\hat{\rho}_1} \right], \quad 1 \leq i \leq K \quad (7)$$

Hence, parameter  $\lambda_i$  should satisfy the following conditions:

$$\sum_{i=1}^K \lambda_i = k = 2^N \quad \text{and } 1 \leq \lambda_i \leq 2^N \quad (8)$$

## C. RESULTS

Validation of the proposed methodology was performed on one-user, two-user, and three-user scenarios. Users with both the same and different power values were tested. For the sake of conciseness, only the following three-user scenarios are illustrated: 1) three users with different power; 2) three users with same power; and 3) three users two of which have

same power. Notably, results from only  $K$ -means clustering algorithm are reported below, since all clustering algorithms performed similarly.

### 1) THREE USERS DIFFERENT POWER

Transmitted power was tuned to assure three users arrived at the fiber-bundle receiver with different power levels. Fig. 3(d) shows that the number of detected peaks in the 1-D histogram function is  $m = 8$ . Hence, “8” is used as input for the clustering algorithms as the number of maximum expected clusters. Results of the clustering techniques are shown in Fig. 5. More specifically, Fig. 5(a) shows the obtained clusters for  $K$ -mean on the received mixed signal  $y[n]$  that was shown in Fig. 3(a). All algorithms produced similar results, namely the ability to identify the same clusters. Fig. 5(b) shows obtained clusters centroids (See red markers in Fig. 5(a)) and the histogram peaks values versus the number of clusters. Results illustrate that the clustering centroids and the histogram peaks values match with only a very small error. However, before defining the number of users, each cluster was assigned a weight  $\rho_i$  with  $1 \leq i \leq 8$  for evaluating if signals are hidden. Cluster weights versus the identified clusters obtained for each algorithm are illustrated in the Fig. 5(c) bar graph. Blue bars show results from fuzzy clustering; orange show hierarchical; yellow represent  $K$ -medoids; and purple represent  $K$ -mean clustering. All bars have comparable cluster heights; accordingly, similar weights ranging from 0.1 to 0.15 were obtained. Moreover, by observing produced weights for each cluster, we were able to conclude that all algorithms performed in a similar way. Reference weight  $\hat{\rho}_i$  was set as expressed in Eq. 6, and the obtained overlapping parameter  $\lambda_i$  where  $1 \leq i \leq 8$  were calculated; results are shown in Fig. 5(d). The illustration shows that each cluster has an overlapping parameter  $\lambda_i = 1$ , indicating there are no hidden signals in the clusters and that all transmitting users have different powers. Thus, given Eq. 8, we obtained  $\sum_{i=1}^8 \lambda_i = \sum_{i=1}^8 1 = 8$ . Knowing that  $8 = 2^N$  and that  $\lambda_i = 1$  for  $1 \leq i \leq 8$ , we can conclude that the number of received users is equal to  $N = \log_2 8 = 3$ .

### 2) THREE USERS WITH SAME POWER

We tuned the transmission power of the laser sources such that at the receiver side two users were received with same power values and the third user with a different power value. Peak detection of the 1D empirical histogram function  $H_L[y_{LF}]$  was performed, and the number of detected peaks in the histogram is  $m = 6$ . This parameter was provided as input to the clustering algorithms as the number of expected clusters. Results of the clustering techniques are shown in Fig. 6. More specifically, Fig. 6(a) shows the obtained six clusters for  $K$ -mean algorithm. Results in Fig. 6(b) illustrate that all clustering algorithms had comparable results and that the cluster centroids matched with peak values obtained from the histogram. Two clusters have a greater number of samples. Accordingly, an overlapping of more than one signal is highly likely. Cluster 2 (See black markers) and cluster 5 (See yellow

markers) have a higher number of samples when compared with other clusters. Eq. 6 suggests that clusters 2 and 5 should outweigh other clusters. Weight analysis was performed and obtained weights for each cluster are shown in Fig. 6(c). Blue bars indicate results from fuzzy clustering; orange for hierarchical; yellow for  $K$ -medoids; and purple for  $K$ -mean clustering.

All clusters had similar weights, ranging from 0.1 to 0.15, except for clusters 2 and 5, which had greater weights ( $\sim 0.25$ ). The overlapping parameter  $\lambda_i$ , where  $1 \leq i \leq 6$ , was computed. See Fig. 6(d). Results indicate that  $\lambda_2 = 2$  and  $\lambda_5 = 2$ , while  $\lambda_i = 1$ , meaning that two signals present in clusters 2 and 5 are hidden. Thus, from Eq. 8,  $\sum_{i=1}^6 \lambda_i = 1 + 2 + 1 + 1 + 2 + 1 = 8$ . Knowing that  $8 = 2^N$ ,  $\lambda_2 = 2$ , and  $\lambda_5 = 2$ , we can conclude that the number of broadcasting users is equal to  $N = \log_2 8 = 3$  and that two users are transmitting with the same power.

### 3) THREE USERS WITH SAME POWER

Finally, given a case where all received users had the same received power, clustering algorithms were able to identify four expected clusters from the peak detection analysis shown in Fig. 4(d); results for  $K$ -means are illustrated in Fig. 7(a). Fig. 7(b) shows that all cluster centroids match extremely well with peak location values obtained in the histogram. Given cluster weights illustrated in Fig. 7(c), it is observed that cluster 2 (See black markers) and cluster 3 (See red markers) outweigh the other two clusters with weights ranging from 0.35 to 0.4. The calculated overlapping parameter  $\lambda_i$  where  $1 \leq i \leq 4$  is shown in Fig. 7(d). Notably,  $\lambda_2 = 3$  and  $\lambda_3 = 3$ , while  $\lambda_1 = 1$  and  $\lambda_4 = 1$ , meaning that three signals are present within clusters 2 and 3. From Eq. 8, we obtained  $\sum_{i=1}^4 \lambda_i = 1 + 3 + 3 + 1 = 8$ . Hence, knowing that  $8 = 2^N$ ,  $\lambda_2 = 3$ , and  $\lambda_3 = 3$ , we concluded that the number of users was equal to  $N = \log_2 8 = 3$  and that three users were received with the same strengths.

### 4) DISCUSSION

The significance of the developed methodology, although it is simple, is its effectiveness to estimate transmitting users regardless of their transmission times; hence no synchronization or prior knowledge of transmission times are required. The algorithm can be implemented at the PHY-layer to continuously monitor power levels and their associated weights to determine the number of users as transmissions get added or dropped asynchronously.

Accuracy analysis was conducted on 45 tested cases to evaluate overall performance of the proposed methodology. Accuracy was defined as the number of cases in which the number of transmitting users was correctly estimated over the total number of studied cases. Results are shown in Table 1. The 45 cases were separated in the following way: 20 for two-user scenarios and 25 for three-user scenarios. High accuracy—greater than 92%—was achieved for all cases.

**TABLE 1.** Accuracy analysis.

NUMBER OF USERS	2	3
ACCURACY	20 100%	25 92%

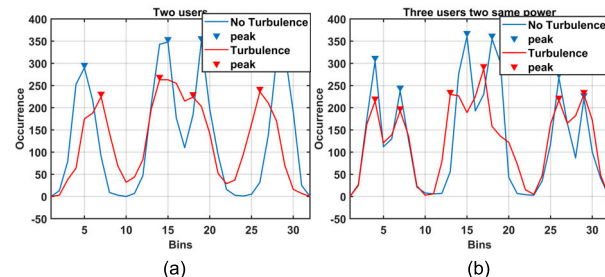


**FIGURE 8.** Turbulence analysis: (a) two users; (b) three users two same power.

### D. TURBULENCE EFFECTS

FSOC can be significantly degraded due to its optical beam atmospheric turbulence sensitivity. Inhomogeneities in atmospheric temperature and pressure lead to random changes in the refractive index, which then cause random variations in the amplitude and phase of optical wave propagating in the turbulent medium. The result is a degraded optical signal [3]. Fluctuation of the received signal intensity (i.e., scintillations [36]) affects FSOC system performance quality and heavily reduces communication performance. The proposed amplitude-based method was evaluated under atmospheric turbulence scenarios. Description of the atmospheric turbulence generation and analysis are detailed in [8]. Received mixed signal under moderate atmospheric turbulence was analyzed. Moderate atmospheric turbulence is characterized by 58.61 °C temperature; 14.21 m/s wind speed; and 80.56% humidity, which resulted in a scintillation index  $\sigma_i^2$  equal to 0.1330 ( $m^2$ ) and refractive index structure constant parameter  $C_n^2$  equal to  $6.19 \cdot 10^{-12}$  ( $m^{-2/3}$ ). Fig. 8 illustrates the peak detection for (a) two users and (b) three users—two of which have the same power for turbulent (See red line) and non-turbulent (See blue line) scenarios. Note that turbulence effect on the empirical distribution of the received mixed signal causes received signal amplitude attenuation and a broadening of obtained peaks. Broadening is clearly visible by comparing peak spacing distances and reduced peak occurrence value of the turbulence compared to non-turbulence. Broadening is primarily due to increasing intensity fluctuations (i.e., temperature and wind); attenuation is mainly caused by the humidity generator (i.e., fog). Weighted clustering analysis was computed, and overlapping parameter  $\lambda_i = 1$  with  $1 \leq i \leq 4$  was calculated for Fig. 8(a) and  $\lambda_1 = \lambda_2 = \lambda_5 = \lambda_6 = 1$  and  $\lambda_3 = \lambda_4 = 2$  were computed for Fig. 8(b). Results shown in Fig. 8(a) and Fig. 8(b) confirm two and three communicating users, respectively.

### V. SAMPLE COMPLEXITY ANALYSIS

Given cluster weight  $\rho_i$  definition in Eq. 3, the number of processed samples represents a fundamental parameter for

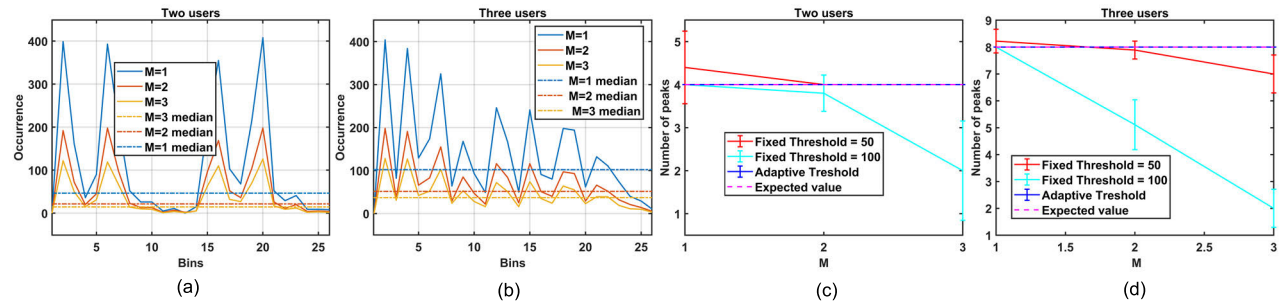


**FIGURE 9. Under-sampling factor M:** (a) two users peak detection; (b) three users peak detection; (c) peaks detection analysis two users; (d) peaks detection analysis three users.

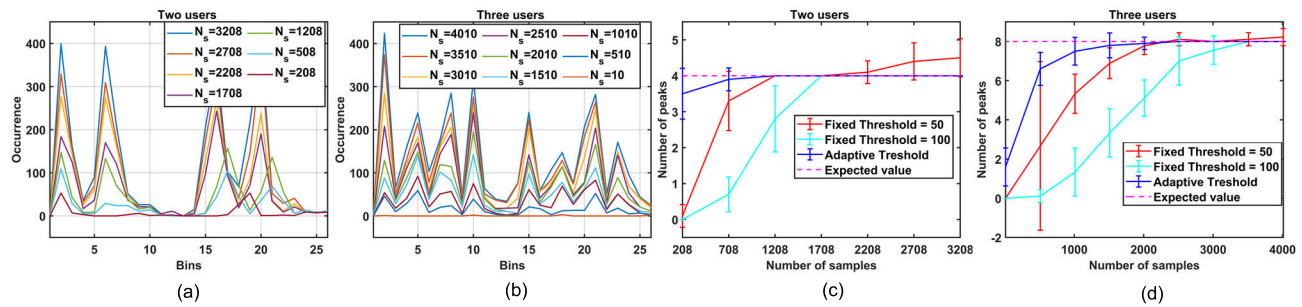


**FIGURE 10. Number of samples  $N_s$ :** (a) two users peak detection; (b) three users peak detection; (c) peaks detection analysis two users; (d) peaks detection analysis three users.

achieving accurate estimation in the proposed methodology. Furthermore, accurate peak detection in the preprocessing analysis (See Eq. 2) is a crucial step for clustering initialization. Optimal threshold selection is pivotal. Experimental analysis for identifying required sample size and receiver sampling rate was conducted to obtain accurate estimation of number of users. The objective was to identify the minimum sample number of the received signals (i.e., preamble signal length) collected and processed with a given receiver sampling rate for accurately detecting histogram peaks of  $H_L[y_{LF}]$  in the pre-processing analysis. Two approaches were experimentally tested—separately and combined: 1) varying sample size  $N_s$  ( $N_s = L$  of Eq. 3) of received signal and 2) varying-sampling reduction factor  $M$  for measuring  $m$  power levels detected at the receiver side in the pre-processing step. These are illustrated in Fig. 3(d) and Fig. 4(d). To perform peak detection (i.e., local maxima of the  $H_L[y_{LF}]$ ), three thresholds were evaluated. Threshold is defined as the level of occurrences in the 1D histogram  $H_L[y_{LF}]$  after a crossed peak is detected. Three evaluated thresholds—50, 100, and adaptive (i.e., median value of  $H_L[y_{LF}]$  occurrence) were chosen. Afterward, a comparison between detected  $m$  and expected peaks  $k$  was computed, where number of expected peaks was  $k = 2^2 = 4$  for two users and  $k = 2^3 = 8$  for three users. Analysis was conducted for one, two, and three users. Results for two- and three-user scenarios are discussed and illustrated in the next sections.

#### A. SAMPLING RATE ANALYSIS

The first analysis decreased the sampling rate of the time series-received mixed signal shown in Fig. 3(a) by a factor  $M$ . Data were collected, and sampling rate reduction was performed as a pre-processing step.  $M = 1, 2, 3$  were tested. Figures 9(a) and 9(b) show the local maxima of the empirical 1-D histogram  $H_L[y_{LF}]$  for  $M = 1, 2$ , and 3 for two and three users, respectively. When comparing results shown in Figures 10(a) and 10(b), one can see that reducing under-sampling factor  $M$  causes the histogram shape to change and the location of detected peaks to shift in a uniform way. This phenomenon is true because samples belonging to each peak are sampled with equal probability. Consequently, peak locations are not shifting much. To define the number of detected peaks, three different thresholds—50, 100, and adaptive—were evaluated. The adaptive threshold is illustrated in Figures 9(a) and 9(b) for each histogram computed at each  $M$  value (See dotted horizontal lines in Fig. 9). Ten acquisitions were collected and detected peak mean values and standard deviations were computed. Fig. 9(c) and Fig. 9(d) illustrate the number of detected peaks obtained with the three thresholds and number of expected peaks (See magenta dotted line) versus the sampling reduction factor  $M$  for two and three users. Given that  $M$  increases, the fixed thresholds underestimated the number of peaks, while the adaptive threshold correctly detected the number of peaks for all tested  $M$  values. To identify the number of samples that nullify the error between detected  $m$  and correct  $k$  number of

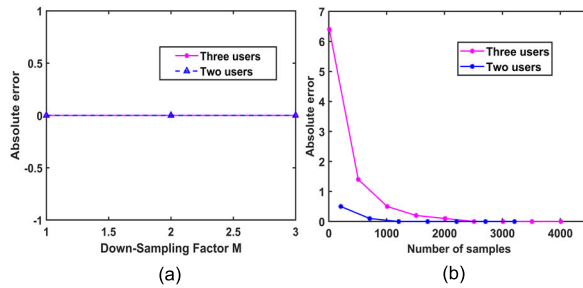


**FIGURE 11.** Absolute error versus (a)  $M$ ; (b)  $N_s$ .

peaks, the absolute error was defined as  $Err = |k - \bar{m}|$  for the adaptive threshold. Computed absolute error is illustrated in Fig. 11(a), which shows that zero error was subsequently obtained for all  $M$  values in both two-(See blue line) and three-(See magenta line) user scenarios.

### B. NUMBER OF SAMPLES ANALYSIS

The second analysis varied number of samples  $N_s$  of the time series received mixed signal for three users, as shown in Fig. 3(a). Starting sample size  $N_s = 3208$  and 4010 samples were used for two- and three-users, respectively. Sample size was consecutively reduced by steps of 500 samples, and the local maxima of empirical 1D histogram  $H_L[y_{LF}]$  were computed, as shown in Figures 10(a) and (b). Similar to the previous case, the histogram shape and the peak locations change; however, this phenomenon occurs in a less uniform way when compared to the previous analysis. Ten acquisitions were collected and processed for each scenario. Mean value and standard deviations of detected peaks were computed. Fig. 10(c) illustrates the number of detected peaks and expected peaks obtained with three thresholds versus sample number  $N_s$  for two users, and Fig. 10(d) shows with three users. Results demonstrate that the adaptive threshold (See blue line) converges faster to the correct number of peaks (See magenta dotted line) than the fixed thresholds. The fixed threshold of 100 (See light blue line) converges to the correct number of peaks slowly, whereas the fixed threshold of 50 (See red line) first converges, and then over-estimates number of peaks. The latter is primarily due to the fact that it might detect small peaks caused by noise. Absolute error was computed, and results show that it is equal to zero, given that the number of analyzed samples is equal to or greater than  $N_s = 1208$  for two users (See blue line) and  $N_s = 2510$  for three users (See magenta line), as shown in Fig. 11(b).

### C. COMBINED ANALYSIS

Finally, a combined analysis of number of samples  $N_s$  with various sampling rate reduction  $M$  was conducted. Figures 12(a) and 12(b) show the number of detected peaks using all three thresholds versus the number of samples for different factors  $M$  for two and three users, respectively. As previously shown in Section V.B, adaptive thresholds (See blue lines) converge faster than fixed thresholds to the correct number of peaks for all tested  $M$ . Fixed threshold 50 (See red line) converges slowly to the correct number of peaks,

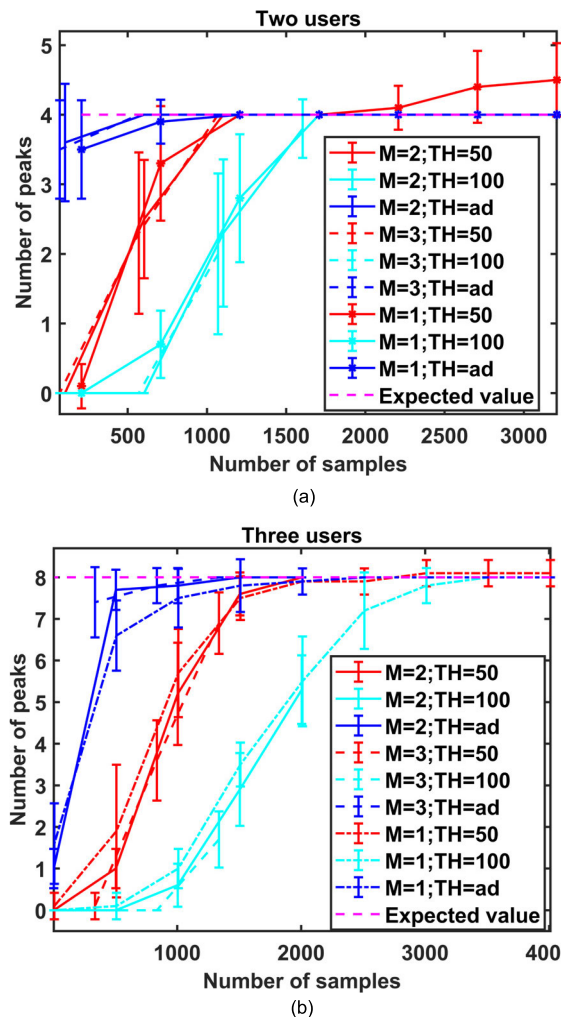


**FIGURE 12.**  $N_s$  and  $M$  analysis: (a) two users; (b) three users.

and then overestimates them, while fixed threshold 100 (See light blue line) converges slower than other thresholds for all tested sampling reduction factors  $M$ . The same behavior was observed for a given threshold and with varying  $M$  values. Sample numbers above which zero error were obtained was considered the minimum number of samples for each sampling rate to obtain an accurate estimation of number of peaks for a three-user scenario (See Fig. 13). As such, those values were employed for the final analysis.

### D. RESULTS

This analysis aimed to derive an empirical equation for predicting the number of required samples, given the receiver sampling rate, for correctly estimating the number of concurrently transmitting users. Nonlinear regression analysis was adopted as the methodology for deriving the function:  $N_{users} = f(N_s, M)$  that best fit data points retrieved and reported in Section V.C. Fig. 14 demonstrates the number of detectable users versus the number of samples required for correct detection when  $M = 1, 2$ , and  $3$  (See red, blue, and black lines, respectively). Both experimental data and obtained fitting curves are illustrated therein. Best fit

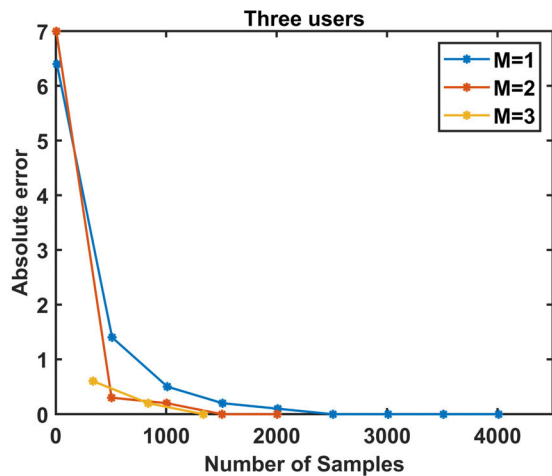


FIGURE 13. Absolute error for three users.

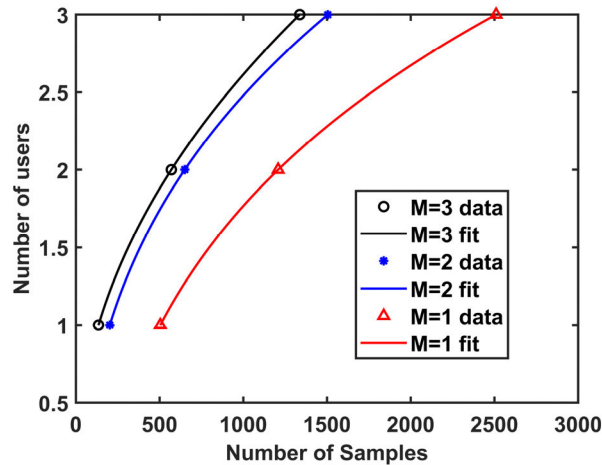


FIGURE 14. Fitting.

TABLE 2. Fitting performance.

	Fitting Performance		
	M=1	M=2	M=3
R-Square	1	1	1

was obtained for each curve using the following power law:  $y = a * x^b + c$ , where  $y$  is the number of users;  $x$  is the number of samples; and  $a, b, c$  are coefficients. Hence, each curve can be mathematically expressed, as follows.

$$N_{users}(N_s, M = i) = a_i * N_s^{b_i} + c_i \quad (9)$$

where  $i = 1, 2, 3$ . Table 2 shows calculated R-square values for evaluating fitting performance. R-square indicates the correlation between response values and predicted response values and also measures the extent of how successful the fit is in explaining data variation.  $R^2 = 1$  was obtained for all cases, meaning that accurate fitting was performed.

Each fitting curve resulted in different parameters  $a_i, b_i, c_i$  for  $i = 1, 2, 3$ , indicating each is a function of the sampling reduction factor  $M$  and, consequently, of receiver sampling

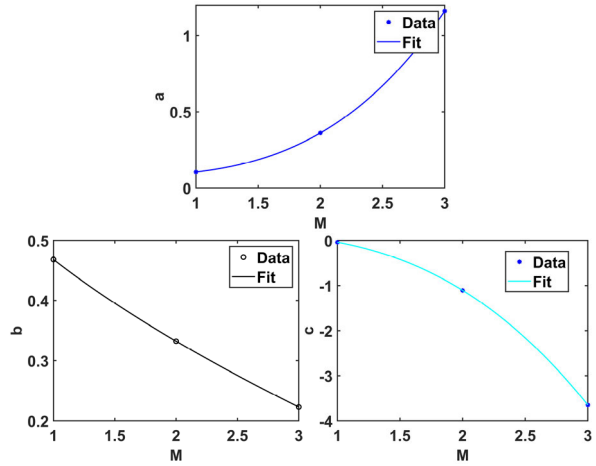


FIGURE 15. Fitting of a, b, c.

rate (See Eq. 9). Therefore, curve fitting was applied on  $a_i, b_i, c_i$  to derive the functions  $a = f(M)$ ,  $b = f(M)$ , and  $c = f(M)$ . Thus, vectors are defined as  $a = [a_1 \ a_2 \ a_3]$ ,  $b = [b_1 \ b_2 \ b_3]$ , and  $c = [c_1 \ c_2 \ c_3]$ . Fitting was performed on these coefficients vectors, as shown in Fig. 15. Power law equation was employed for fitting so that each coefficient could be expressed, as follows.

$$a(M) = a' * M^{b'} + c' \quad (10a)$$

$$b(M) = a'' * M^{b''} + c'' \quad (10b)$$

$$c(M) = a''' * M^{b'''} + c''' \quad (10c)$$

$R^2 = 1$  was obtained for all cases, meaning that accurate fitting was performed for all coefficients. Fig. 15 also shows data points and obtained fitting curves for  $a, b$  and  $c$  vectors. To obtain a final model for prediction, Eq. 9, 10.a, 10.b, and 10.c were combined into the single Eq. 11, which—when provided with receiver sampling rate and number of received and processed samples—indicates how to predict the number of successfully detectable users using the proposed methodology:

$$\begin{aligned} N_{users}(N_s, M) &= a * N_s^b + c \\ &= (a' * M^{b'} + c') * N_s^{(a'' * M^{b''} + c'')} \\ &\quad + a''' * M^{b'''} + c''' \end{aligned} \quad (11)$$

Fig. 16 shows the trend of the predicted  $N_{users}$  for  $M = 1, 2, 3$  and for a range of sample numbers [10:10000], as described in Eq. 11. Since number of users is a discrete parameter, quantization was performed on the predicted  $N_{user}$  values. Obtained results will aid in designing preamble signal length at the head of the packets. For example, if the FSO receiving system is designed to support four simultaneous users with a receiver sampling rate of 1 Gsample/s and required sample size of 5000 samples, then packet length will be designed with a preamble length of 5  $\mu$ s. Moreover, obtained results will be exploited to assist with the design of the electrical and optical receiver system in terms of memory

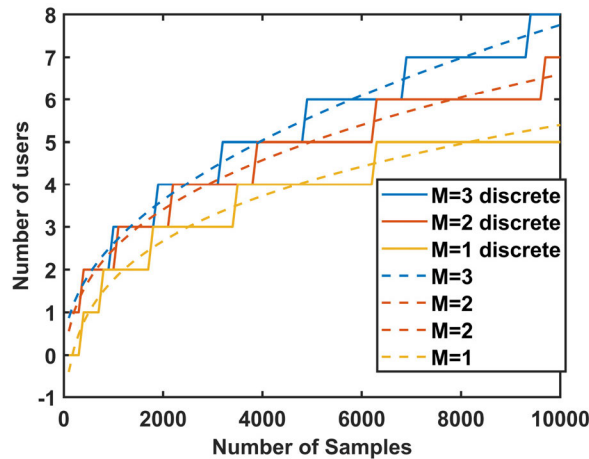


FIGURE 16. Final fitting equation.

requirement and implementation of a cognitive receiver with adaptive sampling rate. The aim is conserving computational complexity and reducing power consumption, which further reduces SWaP system specifications.

## VI. MODEL VALIDATION

To validate the derived empirical model, we employed four users independently and concurrently transmitting into a single receiver (i.e., photodetector) with under sampling factor  $M = 1, 2, 3$ . The applicability of the proposed method in higher data rate communication is presented in this section. 100 Mbps data rate was set for user1; and 150 Mbps for user2; 200 Mbps for user3; and 250 Mbps for user4. All steps detailed in sections IV.A and V.C were applied on the time-series received mixed signals and the minimum number of samples  $N_s$ , which guaranteed accurate peak detection in the obtained empirical 1-D histogram  $H_L[y_{LF}]$  for each  $M$  were identified. The empirical cumulative distribution function (CDF) was calculated to demonstrate validation results. CDF is the probability that the number of samples required to correctly estimate number of communicating users takes a value less than or equal to a given  $N_s$ . Ten acquisitions were considered in the CDF calculation for each  $M$  value; results are illustrated in Fig. 17. The blue, orange, and yellow lines represent the empirical CDFs obtained for  $M = 1, 2, 3$ , respectively. Each point in the CDF represents the minimum number of samples  $N_s$  required to correctly identify  $m = k = 2^4 = 16$  peaks in the  $H_L[y_{LF}]$ . The blue, orange, and yellow dashed vertical lines represent the upper bound  $N_s^*$  for estimating four users, as predicted by Eq. 11 whose trend is illustrated in Fig. 16. The upper bound  $N_s^*$  is defined as  $N_s^* = \{N_s < N_s^* : m = k\}$ , where  $m$  is the number of detected peaks and  $k$  number of expected peaks, as explained in section V.A. Given that all obtained CDF curves are on the left side of the corresponding dashed lines (e.g.,  $N_s < N_s^*$ ), all tested cases could correctly detect four users requiring the number of samples  $N_s$  of the time-series received mixed signals within the predicted region (i.e.,  $N_s < N_s^* = 6200, 3800, 3100$  for four users scenario

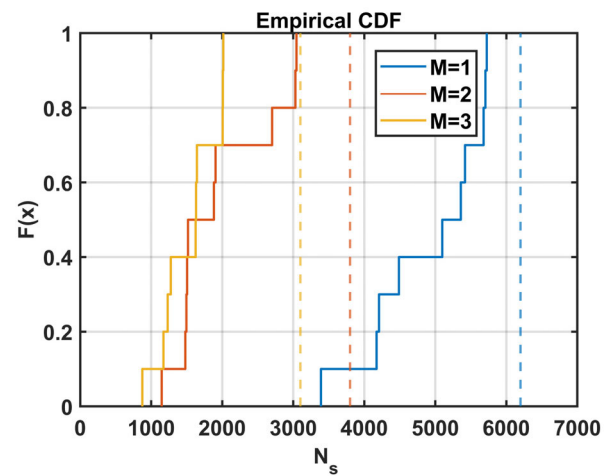


FIGURE 17. Validation results.

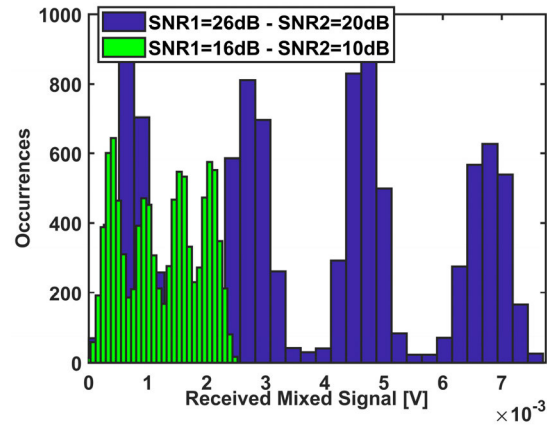


FIGURE 18. Received mixed signals with different dynamic ranges.

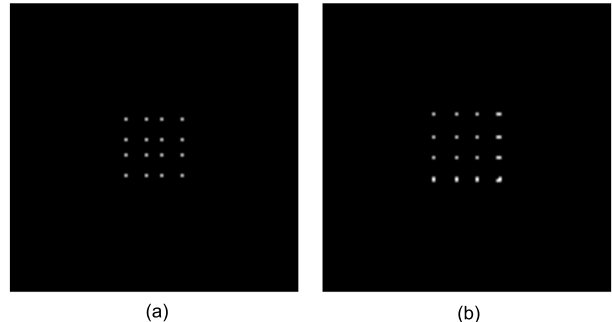


FIGURE 19. (a) 2 users 4-QAM; (b) 1 user 16-QAM.

and for  $M = 1, 2, 3$ , respectively). Experimental results confirm the goodness-of-fit for the derived empirical equation.

## VII. SYSTEM LIMITATIONS

The presented methodology is a power-based technique that uses the amplitude of the received mixed signal to calculate number of simultaneously communicating users. Notably, two factors could affect the proposed method's accuracy and limit system performance.

- 1) *Dynamic range of the received mixed signal.* Fig. 18 shows the histogram  $H_L[y_{LF}]$  of received mixed signals for two transmitting users with diverse SNRs:  $\text{SNR}_1 = 26 \text{ dB}$  and  $\text{SNR}_2 = 20 \text{ dB}$  (See blue histogram); and  $\text{SNR}_1 = 16 \text{ dB}$  and  $\text{SNR}_2 = 10 \text{ dB}$  (See green histogram). Dynamic range of the blue histogram (i.e.,  $\sim 7 \text{ mV}$ ) is wider than the green histogram (i.e.,  $\sim 2 \text{ mV}$ ). The blue histogram  $H_L[y_{LF}]$  can easily accommodate additional users within the dynamic range (i.e., additional peaks within the histogram). Resulting peaks will be clearly separated and easily detected (i.e., there is enough space between two peaks  $\sim 2 \text{ mV}$ ). The green histogram  $H_L[y_{LF}]$  can accommodate fewer users within its dynamic range because additional users will result in an increasing number of merging peaks. The resulting peaks will be difficult to distinguish from one another (i.e., space between two peaks is  $\sim 0.5 \text{ mV}$ ). The higher the dynamic range, the higher the number of users that can be accommodated and detected by the proposed methodology.
- 2) *Multi-level modulation format.* The developed technique has been validated on experimental data using a binary modulation format (i.e., OOK). Given the needs of upcoming optical networks for increased bandwidth and data-rate, multi-level and coherent modulation formats (i.e., QAM) with high-bandwidth efficiency have been under consideration [3]. Extension of the proposed methodology to accommodate multiple modulation formats could consist of applying the technique separately on the real and imaginary part of the received mixed signal. However, the diverse number of users and m-QAM modulation format can result in constellation diagrams with equal symbol distributions. The result is an identical, empirical 1D histogram  $H_L[y_{LF}]$  created from the real and imaginary parts of the received complex signal amplitude. For example, Fig. 19 illustrates the constellation diagram obtained with computer simulations for (a) two users employing 4-QAM and (b) one user with 16-QAM modulation. Given that the modulation format is known at the receiver side, the number of users could be retrieved as  $N = \log_m(p_c)$ , where  $m$  is the modulation order and  $p_c$  is the number of peaks in the constellation diagram. In other words,  $p_c = k_R * k_I$ , where  $k_R$  is the number of detected peaks in  $H_L[\text{Re}\{y_{LF}\}]$  of the real part of the complex received signal and  $k_I$  is the number of detected peaks in  $H_L[\text{Im}\{y_{LF}\}]$  of the imaginary part. It is important to note that if the modulation format is not known, the proposed methodology fails to correctly estimate the number of users.

## VIII. CONCLUSION

Cognitive FSOC networks offer a significant solution for tackling increased system complexity due to heterogeneity of supported services, applications, devices, and transmission

technologies while also guaranteeing high-data rate and bandwidth. In this paper, we proposed a novel methodology for introducing intelligence at the PHY of FSOC networks to estimate number of concurrently transmitting users sharing time, bandwidth, and space resources. The proposed technique leverages unsupervised ML on the amplitude information of the received mixed signals. Four clustering techniques, namely  $K$ -mean, hierarchical,  $K$ -medoid and fuzzy clustering, were experimentally validated in a setup composed of a fiber-bundle receiver, in which one, two, and three independent transmitting users were tested. Moreover, a weighted clustering analysis was proposed to correct for underestimation when users with the same power values are received. Experimental results proved that the proposed technique can successfully estimate the number of transmitting users, even under moderate atmospheric turbulence.

Large data set scalability has become a challenging issue for clustering algorithms. Existing clustering algorithms require scalable solutions to manage large datasets in order to avoid high computational complexity. A further investigation aimed to identify minimum data size and a receiver sampling rate for successfully estimating the number of users leveraging the proposed methodology. Effect of sample size and receiver sampling rate on the estimation accuracy were experimentally tested and evaluated. Finally, an empirical equation for successfully predicting the number of detectable users, given the number of samples and receiver sampling rate, was derived and validated with data collected from four communicating users.

Future work will aim at investigating and implementing new cognitive capabilities for OWC applications, as follows.

- 1) Implementation of the presented methodology to process non-synchronous transmissions (new signal arrival and departure); 2) Method modification to overcome limitations described in section VI; 3) Investigation of a supervised-ML analysis to estimate QoT parameters (e.g., SNR, SINR, BER, etc.).

## REFERENCES

- [1] M. Z. Chowdhury, M. T. Hossan, A. Islam, and Y. M. Jang, "A comparative survey of optical wireless technologies: Architectures and applications," *IEEE Access*, vol. 6, pp. 9819–9840, 2018.
- [2] M. A. Khalighi and M. Uysal, "Survey on free space optical communication: A communication theory perspective," *IEEE Commun. Surveys Tuts.*, vol. 16, no. 4, pp. 2231–2258, 4th Quart., 2014.
- [3] H. Kaushal and G. Kaddoum, "Optical communication in space: Challenges and mitigation techniques," *IEEE Commun. Surveys Tuts.*, vol. 19, no. 1, pp. 57–96, 1st Quart., 2017.
- [4] B. Moision, B. Erkmen, E. Keyes, T. Belt, O. Bowen, D. Brinkley, P. Csonka, M. Eglington, A. Kazmierski, N.-H. Kim, J. Moody, T. Tu, and W. Vermeer, "Demonstration of free-space optical communication for long-range data links between balloons on project loon," *Proc. SPIE*, vol. 10096, Feb. 2017, Art. no. 100960Z.
- [5] E. A. Park, D. Cornwell, and D. Israel, "NASA's next generation  $\geq 100 \text{ gbps}$  optical communications relay," in *Proc. IEEE Aerosp. Conf.*, Mar. 2019, pp. 1–9.
- [6] Y. Kaymak, R. Rojas-Cessa, J. Feng, N. Ansari, M. Zhou, and T. Zhang, "A survey on acquisition, tracking, and pointing mechanisms for mobile free-space optical communications," *IEEE Commun. Surveys Tuts.*, vol. 20, no. 2, pp. 1104–1123, 2nd Quart., 2018.

- [7] T. Rakia, F. Gebali, H.-C. Yang, and M.-S. Alouini, "Throughput analysis of point-to-multi-point hybrid FSO/RF network," in *Proc. IEEE Int. Conf. Commun. (ICC)*, May 2017, pp. 1–6.
- [8] F. Aveta, H. H. Refai, and P. LoPresti, "Multiple access technique in a high-speed free-space optical communication link: Independent component analysis," *Opt. Eng.*, vol. 58, no. 3, p. 1, Mar. 2019.
- [9] A. Kaadan, H. H. Refai, and P. G. LoPresti, "On the development of modular optical wireless elements (MOWE)," in *Proc. IEEE Globecom Workshops (GC Wkshps)*, Dec. 2015, pp. 1–7.
- [10] A. Kaadan, H. Refai, and P. LoPresti, "Wide-area and omnidirectional optical detector arrays using modular optical elements," *Appl. Opt.*, vol. 55, no. 18, pp. 4791–4800, 2016.
- [11] P. LoPresti, N. Hutchins, S. Kohrmann, M. F. Babelli, and H. H. Refai, "Wavelength dependence of a fiber-bundle based FSO link," in *Proc. IEEE Globecom Workshops (GC Wkshps)*, Dec. 2014, pp. 493–498.
- [12] P. LoPresti, S. Kohrmann, D. Buchheim, J. Rodriguez, M. F. Babelli, and H. H. Refai, "Performance analysis of a fiber-bundle based FSO link," in *Proc. IEEE Int. Conf. Commun. (ICC)*, Jun. 2015, pp. 5091–5097.
- [13] F. Aveta, H. H. Refai, and P. LoPresti, "Multi-user detection in optical wireless communication," in *Proc. 15th Int. Wireless Commun. Mobile Comput. Conf. (IWCMC)*, Jun. 2019, pp. 214–219.
- [14] F. Aveta, H. H. Refai, and P. LoPresti, "Multi-user FSO communication link," in *Proc. Cognit. Commun. Aerosp. Appl. Workshop (CCAA)*, Jun. 2017, pp. 1–5.
- [15] F. Aveta, H. H. Refai, P. LoPresti, S. A. Tedder, and B. L. Schoenholz, "Independent component analysis for processing optical signals in support of multi-user communication," *Proc. SPIE*, vol. 10524, Feb. 2018, Art. no. 105241D.
- [16] F. Aveta and H. H. Refai, "Free space optical non-orthogonal multiple access experimentation," in *Proc. Free-Space Laser Commun. XXXI*, Mar. 2019, p. 60.
- [17] F. Musumeci, C. Rottondi, A. Nag, I. Macaluso, D. Zibar, M. Ruffini, and M. Tornatore, "An overview on application of machine learning techniques in optical networks," *IEEE Commun. Surveys Tuts.*, vol. 21, no. 2, pp. 1383–1408, 2nd Quart., 2018.
- [18] F. N. Khan, Q. Fan, C. Lu, and A. P. T. Lau, "An optical Communication's perspective on machine learning and its applications," *J. Lightw. Technol.*, vol. 37, no. 2, pp. 493–516, Jan. 15, 2019.
- [19] J. Mata, I. de Miguel, R. J. Durán, N. Merayo, S. K. Singh, A. Jukan, and M. Chamanian, "Artificial intelligence (AI) methods in optical networks: A comprehensive survey," *Opt. Switching Netw.*, vol. 28, pp. 43–57, Apr. 2018.
- [20] I. I. R. H. Brumley, R. H. Brumley III, R. Rosenthal, S. Birrell, M. J. Reedy, and F. W. Brumley, "Optical communication system," U.S. Patents, 20202114038 A1, Jan. 28, 2020.
- [21] F. Aveta, H. H. Refai, and P. G. LoPresti, "Number of users detection in multi-point FSOC using unsupervised machine learning," *IEEE Photon. Technol. Lett.*, vol. 31, no. 22, pp. 1811–1814, Nov. 15, 2019.
- [22] S. Hanneke, "The optimal sample complexity of PAC learning," *J. Mach. Learn. Res.*, vol. 17, no. 1, pp. 1319–1333, 2016.
- [23] W. Mo, Y.-K. Huang, S. Zhang, E. Ip, D. C. Kilper, Y. Aono, and T. Tajima, "ANN-based transfer learning for QoT prediction in real-time mixed line-rate systems," in *Proc. Opt. Fiber Commun. Conf.*, 2018, pp. 1–3.
- [24] L. Barletta, A. Giusti, C. Rottondi, and M. Tornatore, "QoT estimation for unestablished lightpaths using machine learning," in *Proc. Opt. Fiber Commun. Conf.*, 2017, pp. 1–3.
- [25] T. Tanimura, T. Hoshida, J. C. Rasmussen, M. Suzuki, and H. Morikawa, "OSNR monitoring by deep neural networks trained with asynchronously sampled data," in *Proc. 21st Optoelectron. Commun. Conf. (OECC) Held Jointly Int. Conf. Photon. Switching (PS)*, 2016, pp. 1–3.
- [26] S. Aladin and C. Tremblay, "Cognitive tool for estimating the QoT of new lightpaths," in *Proc. Opt. Fiber Commun. Conf.*, 2018, pp. 1–3.
- [27] P.-N. Tan, M. Steinbach, and V. Kumar, *Introduction to Data Mining*. London, U.K.: Pearson, 2016.
- [28] T. S. R. Shen, K. Meng, A. P. T. Lau, and Z. Y. Dong, "Optical performance monitoring using artificial neural network trained with asynchronous amplitude histograms," *IEEE Photon. Technol. Lett.*, vol. 22, no. 22, pp. 1665–1667, Nov. 15, 2010.
- [29] F. N. Khan, T. S. R. Shen, Y. Zhou, A. P. T. Lau, and C. Lu, "Optical performance monitoring using artificial neural networks trained with empirical moments of asynchronously sampled signal amplitudes," *IEEE Photon. Technol. Lett.*, vol. 24, no. 12, pp. 982–984, Jun. 2012.
- [30] T. Tanimura, T. Hoshida, T. Kato, S. Watanabe, and H. Morikawa, "Data-analytics-based optical performance monitoring technique for optical transport networks," in *Proc. Opt. Fiber Commun. Conf.*, 2018, pp. 1–3.
- [31] N. G. Gonzalez, D. Zibar, and I. T. Monroy, "Cognitive digital receiver for burst mode phase modulated radio over fiber links," in *Proc. 36th Eur. Conf. Exhib. Opt. Commun.*, Sep. 2010, pp. 1–3.
- [32] D. Wang, M. Zhang, Z. Li, J. Li, M. Fu, Y. Cui, and X. Chen, "Modulation format recognition and OSNR estimation using CNN-based deep learning," *IEEE Photon. Technol. Lett.*, vol. 29, no. 19, pp. 1667–1670, Oct. 1, 2017.
- [33] J. Thrane, J. Wass, M. Piels, J. C. M. Diniz, R. Jones, and D. Zibar, "Machine learning techniques for optical performance monitoring from directly detected PDM-QAM signals," *J. Lightw. Technol.*, vol. 35, no. 4, pp. 868–875, Feb. 15, 2017.
- [34] A. K. Majumdar, *Advanced Free Space Optics (FSO): A Systems Approach*, vol. 186. New York, NY, USA: Springer, 2014.
- [35] T. Chen and H. Ren Wu, "Impulse noise removal by multi-state median filtering," in *Proc. IEEE Int. Conf. Acoust., Speech, Signal Process.*, Jun. 2000, pp. 2183–2186.
- [36] A. Malik and P. Singh, "Free space optics: Current applications and future challenges," *Int. J. Opt.*, vol. 2015, pp. 1–7, Sep. 2015.



**FEDERICA AVETA** (Member, IEEE) received the B.S. and M.Sc. degrees in electronics engineering from La Sapienza University, Rome, Italy, in 2012 and 2016, respectively. She is currently pursuing the Ph.D. degree with the Electrical and Computer Engineering Department, The University of Oklahoma, Tulsa. Her research interests include optical communication, free space optics, and machine learning application in optical communication.



**HAZEM H. REFAI** (Member, IEEE) received the M.S.E.E. and Ph.D. degrees from The University of Oklahoma (OU), Norman, in 1993 and 1999, respectively. He currently serves as an Associate Professor with the OU Department of Electrical and Computer Engineering Telecommunication Program, Tulsa, OK, USA. He is the Founder and Director of the OU's Wireless Electromagnetic Compliance and Design Center, where he and his team focus on basic and applied research in radiofrequency (RF) and optical wireless communication and networks, as well as electromagnetic compatibility. His research interests include the development of physical and medium-access control layers for mobile laser communication networks using free space optics, cognitive radios and networks, sensor-based auto collision avoidance systems, vehicle-to-vehicle communication protocols, and portable hybrid RF/free-space-optical communication systems for disaster recovery.



**PETER G. LOPRESTI** (Member, IEEE) received the B.S.E. degree in electrical engineering from the University of Delaware, Newark, in 1988, and the Ph.D. degree in electrical engineering from Pennsylvania State University, University Park, in 1994. He currently serves as a Professor of Electrical Engineering with The University of Tulsa, Tulsa, OK, USA. He is also the Director of the Williams Communications Optical Networking Laboratory, Department of Electrical Engineering, The University of Tulsa, and a project consultant for a company developing 3-D displays. His research interests include optical communication systems engineering, mobile free-space optical communication network design and implementation for disaster recovery, environmental monitoring, battlefield communication, and optical sensor development for environmental monitoring.